Supporting Information

Cation-exchange and oxygen vacancies triggered capacity in hierarchical α-$Ni_{1-x}Cu_xMoO_4$@CC flexible electrodes for energy-storage applications

Sk. Khaja Hussain,[†, ‡, #] *B. N. Vamsi Krishna,*[†, #] *and Jae Su Yu* [†, *]

[†]*Department of Electronic Engineering, Institute for Wearable Convergence Electronics, Kyung Hee University, 1 Seocheon-dong, Giheung-gu, Yongin-si, Gyeonggi-do 446-701, Republic of Korea*

[‡]*Nanosensor Research Institute, Hanyang University, 55 Hanyangdaehak-ro, Sangnok-gu, Ansan, Gyeonggi-do 15588, Republic of Korea*

Author Information

[#] *S.K.H. and B.N.V.K contributed equally to this work.*

**Corresponding author*

E-mail: jsyu@khu.ac.kr

Chemicals and material characterizations

The chemicals of nickel acetate ($Ni(CH_3CO_2)_2 \cdot 4H_2O$), copper acetate ($Cu(CH_3CO_2)_2 \cdot xH_2O$), and ammonium molybdate tetrahydrate ($(NH_4)_6Mo_7O_{24} \cdot 4H_2O$) were purchased by Sigma Aldrich Co., South Korea. Polyvinylidene fluoride (PVDF; $-(C_2H_2F_2)n-$) and N-methyl-2-pyrrolidone (NMP; C_5H_9NO) were received from Daejung Chemicals Ltd., South Korea. The above chemicals were utilized in our experiments without any alterations in their purity.

The electrode samples were characterized by X-ray diffraction (XRD) analysis (Cu Kα (λ = 1.54056 Å)) through the Mac Science M18XHF-SRA instrument to find out the pure crystallinity. High-resolution Raman spectroscopy (Research Leica DM250) with 514 nm laser excitation was used to measure the Raman spectra of the electrodes. Field-emission scanning electron microscope (FE-SEM; LEO SUPRA 55 Carl Zeiss) equipped with energy-dispersive X-ray spectroscopy (EDS) was used to investigate the surface morphologies of the electrodes. X-ray photoelectron spectroscopy (XPS; Thermo Multi-Lab 2000 System) was employed to identify the charges of the metal ions. Electron paramagnetic resonance spectroscopy (Bruker (EMXplus-9.5/2.7) was employed to identify the oxygen vacancies.

Electrochemical analysis

The electrochemical data for the flexible α-$NiMoO_4$@carbon cloth (CC) and α-$Ni_{1-x}Cu_xMoO_4$@CC (x = 1, 3, 5, and 7 mol%) electrodes were collected by IviumStat; IVIUM Technologies instrument in a three-electrode electrochemical system (25 °C). The loading masses of the materials on the CC in a 1 × 1 cm^2 area were ~3.1 ± 0.05 mg cm^{-2} referred to as a working electrode. Ag/AgCl is the reference electrode and Pt wire is the counter electrode.

Before electrochemical analysis, a freshly made 1 M aqueous KOH electrolyte solution was used.

Table S1. Three-electrode electrochemical performance and two-electrode stability, energy, and power density comparisons of the designed α-$Ni_{0.95}Cu_{0.05}MoO_4$@CC electrode and FHS device with the previously published reports of molybdenum and nickel-based composites.

Composite material	Preparation method	Electro lyte	Three-electrode performance	Cycling stability @ Retention	Energy and power densities	Ref.
$CoMoO_4$-$NiMoO_4$ NTs	Two-step hydrothermal method	3 M KOH	751 F g^{-1} at 1 A g^{-1}	2000 cycles @ (94%)	E (30.86 Wh kg^{-1}) P (4.85 kW kg^{-1})	S1
Carbon sphere@$NiMoO_4$	A hydrothermal method	2M NaOH	268.8 F g^{-1} at 1 A g^{-1}	2000 cycles @ (88.4%)	-	S2
$NiMoO_4$-PANI nanocomposite	A solvothermal method	PVA-KOH gel electrol yte	1214 F g^{-1} at 1 A g^{-1}	5000 cycles @ (98.6%)	E (30.07 Wh kg^{-1}) P (240 W kg^{-1})	S3
$NiMoO_4$ nanorods	A facile solvothermal method	3 M KOH	670 F g^{-1} at 0.3 A g^{-1}	3000 cycles @ (88%)	-	S4
$NiMoO_4$/$CoMoO_4$ nanorod arrays	Hydrothermal and electrochemical deposition methods	1 M KOH	778.1 F g^{-1} at 0.5 A g^{-1}	-	E (33.1 Wh kg^{-1}) P (3195 W kg^{-1})	S5
$NiMoO_4$ nanorods on Ni foam	Hydrothermal route	6 M KOH	594 F g^{-1} at 1 A g^{-1}	1000 cycles @ (56%)	E (18 Wh kg^{-1}) P (704 W kg^{-1})	S6
$NiMoO_4$ nanospheres on Ni-foam	Hydrothermal route	3 M KOH	974.4 F g^{-1} at 1 A g^{-1}	2000 cycles @ 5 A g^{-1}	E (20.1 Wh kg^{-1}) P (2100 W kg^{-1})	S7

$NiMoO_4$-Ag/rGO	Hydrothermal route	6 M KOH	566.4 C g^{-1} at 1 A g^{-1}	8000 cycles @ (73.3%)	E (40.98 Wh kg^{-1}) P (800 W kg^{-1})	S8
$CoMoO_4$-$NiMoO_4$ Nanotubes	Hydrothermal method	2 M KOH	1079 F g^{-1} at 5 A g^{-1}	1000 cycles @ (98.4%)	E (33 Wh kg^{-1}) P (6000 W kg^{-1})	S9
$CoMoO_4$-$NiMoO_4 \cdot xH_2O$	Chemical co-precipitation	2 M KOH	1039 F g^{-1} at 2.5 mA cm^{-2}	1000 cycles @ (75.1%)	-	S10
$NiMoO_4$@NiS_2/ MoS_2	Hydrothermal method	6 M KOH	970 F g^{-1} at 5 A g^{-1}	5000 cycles @ (60%)	E (26.8 Wh kg^{-1}) P (700 W kg^{-1})	S11
MoO_3 nanobelts	A facile hydrothermal method	0.5 M Li_2SO_4	369 F g^{-1} at 0.1 A g^{-1}	500 cycles @ (95%)	-	S12
MoO_3 nanorods	A facile hydrothermal method	1 M Na_2SO_4	214 F g^{-1} at 0.1 A g^{-1}	1000 cycles @ (71.7%)	-	S13
Layered MoO_3@C	Calcination process	1 M H_2SO_4	331 F g^{-1} at 1 A g^{-1}	1000 cycles @ (87.9%)	-	S14
rGO-wrapped MoO_3 composites	A novel and simple method	1 M H_2SO_4	617 F g^{-1} at 1 A g^{-1}	6000 cycles @ (87.5%)	-	S15
ZnO@MoO_3 core/shell nanocables	A simple electrochemical method	1 M Na_2SO_4	236 F g^{-1} at 5 mV s^{-1}	1000 cycles @ (90%)	-	S16

MoO_3@PANI nanobelts	A simple and green approach	1 M H_2SO_4	714 F g^{-1} at 1 mV s^{-1}	3000 cycles @ (76.7%)	-	S17
WS_2/α-$NiMoO_4$	Microwave hydrothermal and calcination processes	-	460 F g^{-1} at 1 A g^{-1}	2000 cycles @ (92%)	-	S18
NCSe@NMO@rGO-NF	Hydrothermal method	2 M KOH	396.1 mAh g^{-1} at 1 A g^{-1}	8000 cycles @ (89.4%)	E (63.2 Wh kg^{-1}) P (7983.5 W kg^{-1})	S19
$NiMoO_4$ arrays	Hydrothermal and calcination method	2 M KOH	-	4000 cycles @ (73.4%)	E (53.8 Wh kg^{-1}) P (239 W kg^{-1})	S20
$CoMoO_4$@$NiMoO_4$ core-shell nanosheet arrays	A facile two-step hydrothermal method	2 M KOH	-	3000 cycles @ (95%)	E (28.7 Wh kg^{-1}) P (267 W kg^{-1})	S21
$NiMoO_4$ nanoparticles//AC	Calcination	6 M KOH	1438 F g^{-1} at 1 A g^{-1}	3000 cycles @ (92%)	E (30 Wh kg^{-1}) P (403 W kg^{-1})	S22
Co_3O_4@$NiMoO_4$ NSA//AC	Hydrothermal reaction	2 M KOH	1526 F g^{-1} at 3 mA cm^{-2}	-	E (37.8 Wh kg^{-1}) P (482 W kg^{-1})	S23
$NiMoO_4$	Hydrothermal in situ diffusion reaction	2 M KOH	864 F g^{-1} at 1 A g^{-1}	1000 cycles @ (71%)	-	S24
$CoMoO_4$-$NiMoO_4 \cdot xH_2O$	Chemical co-precipitation method	2 M KOH	1039 F g^{-1} at 2.5 mA cm^{-2}	1000 cycles @ (72.3%)	-	S25

P-doped $Co_{0.21}Ni_{0.79}MoO_4$-n	Calcination	2 M KOH	1127 F g^{-1} at 0.5 A g^{-1}	-	E (49.2 Wh kg^{-1}) P (747.7 W kg^{-1})	S26
PCNS@$Co_xNi_{1-x}MoO_4$	A hydrothermal process	2 M KOH	1127 F g^{-1} at 0.5 A g^{-1}	5000 cycles @ (101%)	E (36.7 Wh kg^{-1}) P (346.4 W kg^{-1})	S27
Co_3O_4@$NiMoO_4$ flower-like hybrid arrays	Hydrothermal and post-annealing treatment	2 M KOH	636.8 C g^{-1} at 5 mA cm^{-2}	2000 cycles @ (84.1%)	E (58.5 Wh kg^{-1}) P (389 W kg^{-1})	S28
MoO_3 hybrids	A sol–gel method	1 M H_2SO_4	135 F g^{-1} at 1.3 A g^{-1}	1000 cycles @ (82%)	-	S29
$CoMoO_4$@PPy NHs	-	2 M KOH	1203 F g^{-1} at 2 A g^{-1}	5000 cycles @ (96%)	E (40.3 Wh kg^{-1}) P (749 W kg^{-1})	S30
$NiMoO_{4-x}$@C	An annealing process	2 M KOH	1720 F g^{-1} at 1 mA cm^{-2}	6000 cycles @ (84.5%)	E (51.6 Wh kg^{-1}) P (203.95 W kg^{-1})	S31
α-$Ni_{0.95}Cu_{0.05}MoO_4$ @CC	**A facile hydrothermal method**	**1 M KOH**	**342 C g^{-1} (1088 F g^{-1}) at 1 A g^{-1}**	**FAS device @10000 cycles (91%)**	**E (83 Wh kg^{-1}) P (10.5 kW kg^{-1})**	**Present Work**

References

S1. Q. Yang and S.-Y. Lin, *RSC Adv.*, 2016, **6**, 10520-10526.

S2. C. Wei, Y. Huang, J. Yan, X. Chen and X. Zhang, *Ceram. Int.*, 2016, **42**, 15694-15700.

S3. H. Gao, F. Wu, X. Wang, C. Hao and C. Ge, *Int. J. Hydrogen Energy*, 2018, **43**, 18349-18362.

S4. E. R. Ezeigwe, P. S. Khiew, C. W. Siong, I. Kong and M. T. T. Tan, *Ceram. Int.*, 2017, **43**, 13772-13780.

S5. B. Yu, G. Jiang, W. Xu, C. Cao, Y. Liu, N. Lei, U. Evariste and P. Ma, *J. Alloys Compd.*, 2019, **799**, 415-424.

S6. N. S. Neeraj, B. Mordina, A. K. Srivastava, K. Mukhopadhyay and N. E. Prasad, *Appl. Surf. Sci.*, 2019, **473**, 807-819.

S7. D. Cai, D. Wang, B. Liu, Y. Wang, Y. Liu, L. Wang, H. Li, H. Huang, Q. Li and T. Wang, *ACS Appl. Mater. Interfaces*, 2013, **5**, 12905-12910.

S8. B. Huang, D. Yao, J. Yuan, Y. Tao, Y. Yin, G. He and H. Chen, *J. Colloid Interface Sci.*, 2022, **606**, 1652-1661.

S9. Z. Yin, Y. Chen, Y. Zhao, C. Li, C. Zhu and X. Zhang, *J. Mater. Chem. A*, 2015, **3**, 22750-22758.

S10. M.-C. Liu, L.-B. Kong, C. Lu, X.-J. Ma, X.-M. Li, Y.-C. Luo and L. Kang, *J. Mater. Chem. A*, 2013, **1**, 1380-1387.

S11. D. Chen, M. Lu, L. Li, D. Cai, J. Li, J. Cao and W. Han, *J. Mater. Chem. A*, 2019, **7**, 21759-21765.

S12. J. Jiang, J. Liu, S. Peng, D. Qian, D. Luo, Q. Wang, Z. Tian and Y. Liu, *J. Mater. Chem. A*, 2013, **1**, 2588-2594.

S13. Z. Cui, W. Yuan and C. M. Li, *J. Mater. Chem. A*, 2013, **1**, 12926-12931.

S14. H. Ji, X. Liu, Z. Liu, B. Yan, L. Chen, Y. Xie, C. Liu, W. Hou and G. Yang, *Adv. Funct. Mater.*, 2015, **25**, 1886-1894.

S15. X. Cao, B. Zheng, W. Shi, J. Yang, Z. Fan, Z. Luo, X. Rui, B. Chen, Q. Yan and H. Zhang, *Adv. Mater.*, 2015, **27**, 4695-4701.

S16. G.-R. Li, Z.-L. Wang, F.-L. Zheng, Y.-N. Ou and Y.-X. Tong, *J. Mater. Chem.*, 2011, **21**, 4217-4221.

S17. F. Jiang, W. Li, R. Zou, Q. Liu, K. Xu, L. An and J. Hu, *Nano Energy*, 2014, **7**, 72-79.

S18. S. K. Ray, B. Pant, M. Park, J. Hur and S. W. Lee, *Ceram. Int.*, 2020, **46**, 19022-19027.

S19. J. Acharya, B. Pant, G. P. Ojha and M. Park, *J. Mater. Chem. A*, 2022, **10**, 7999-8014.

S20. C. Qing, Y. Liu, X. Sun, X. OuYang, H. Wang, D. Sun, B. Wang, Q. Zhou, L. Xu and Y. Tang, *RSC Adv.*, 2016, **6**, 67785-67793.

S21. Z. Zhang, H. Zhang, X. Zhang, D. Yu, Y. Ji, Q. Sun, Y. Wang and X. Liu, *J. Mater. Chem. A*, 2016, **4**, 18578-18584.

S22. V. S. Budhiraju, R. Kumar, A. Sharma and S. Sivakumar, *Electrochim. Acta*, 2017, **238**, 337-348.

S23. W. Hong, J. Wang, P. Gong, J. Sun, L. Niu, Z. Yang, Z. Wang and S. Yang, *J. Power Sources*, S2014, **270**, 516-525.

S24. Z. Yin, S. Zhang, Y. Chen, P. Gao, C. Zhu, P. Yang and L. Qi, *J. Mater. Chem. A*, 2015, **3**, 739-745.

S25. M.-C. Liu, L.-B. Kong, C. Lu, X.-J. Ma, X.-M. Li, Y.-C. Luo and L. Kang, *J. Mater. Chem. A*, 2013, **1**, 1380-1387.

S26. T. Xing, Y. Ouyang, Y. Chen, L. Zheng, C. Wu and X. Wang, *J. Energy Storage*, 2020, **28**, 101248.

S27. J. Lin, L. Yao, Z. Li, P. Zhang, W. Zhong, Q. Yuan and L. Deng, *Nanoscale*, 2019, **11**, 3281-3291.

S28. Y. Zhang, Y. Yang, L. Mao, D. Cheng, Z. Zhan and J. Xiong, *Mater. Lett.*, 2016, **182**, 298-301.

S29. Q. Mahmood, W. S. Kim and H. S. Park, *Nanoscale*, 2012, **4**, 7855-7860.

S30. A. Liu and J. Tang, *Ceram. Int.*, 2020, **46**, 10893-10902.

S31. P. Wang, X. Ding, R. Zhe, T. Zhu, C. Qing, Y. Liu and H.-E. Wang, *Nanomater.*, 2022, **12**, 1094.

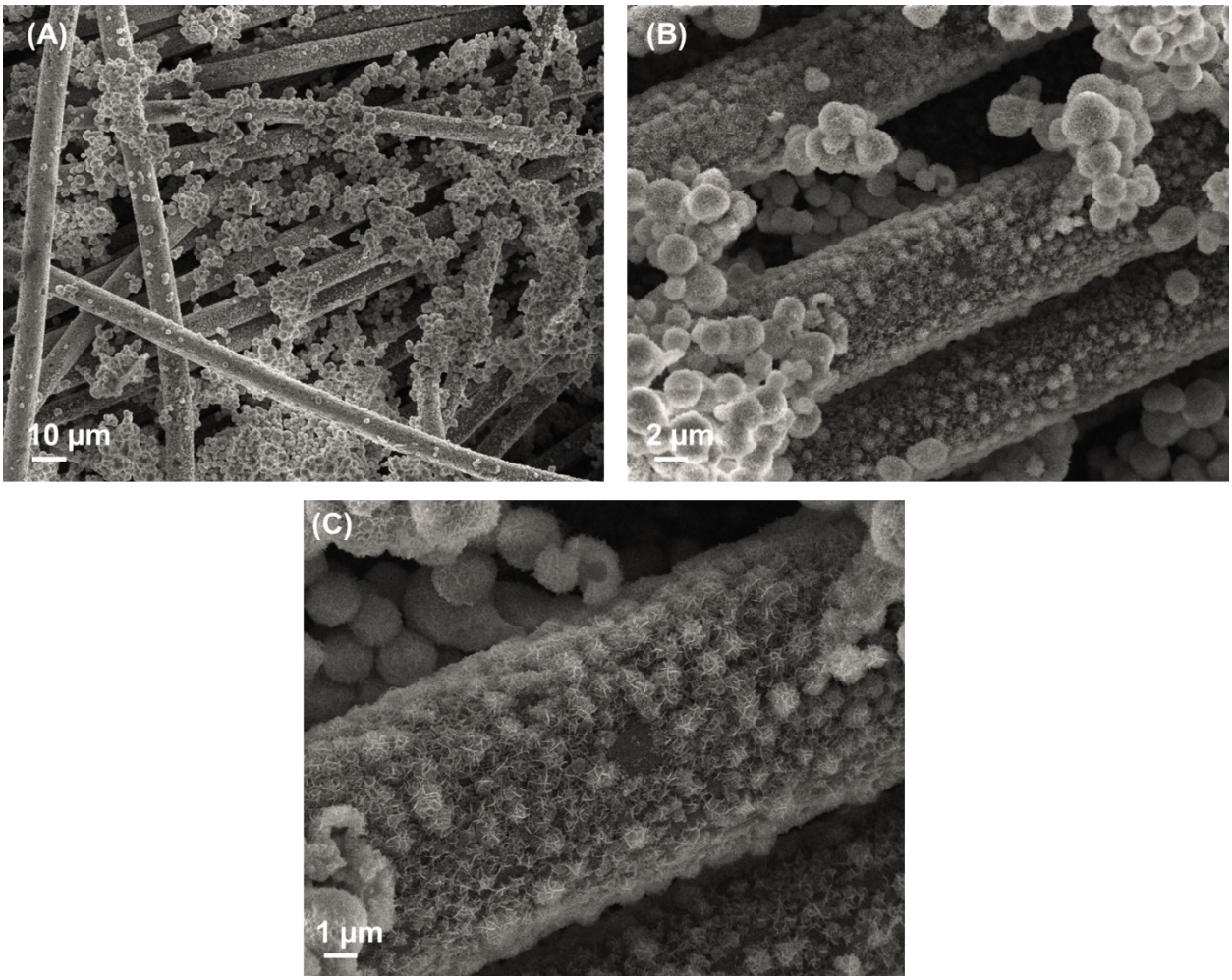

Fig. S1. (A-C) FE-SEM images of α-$Ni_{0.93}Cu_{0.07}MoO_4$@CC electrode.

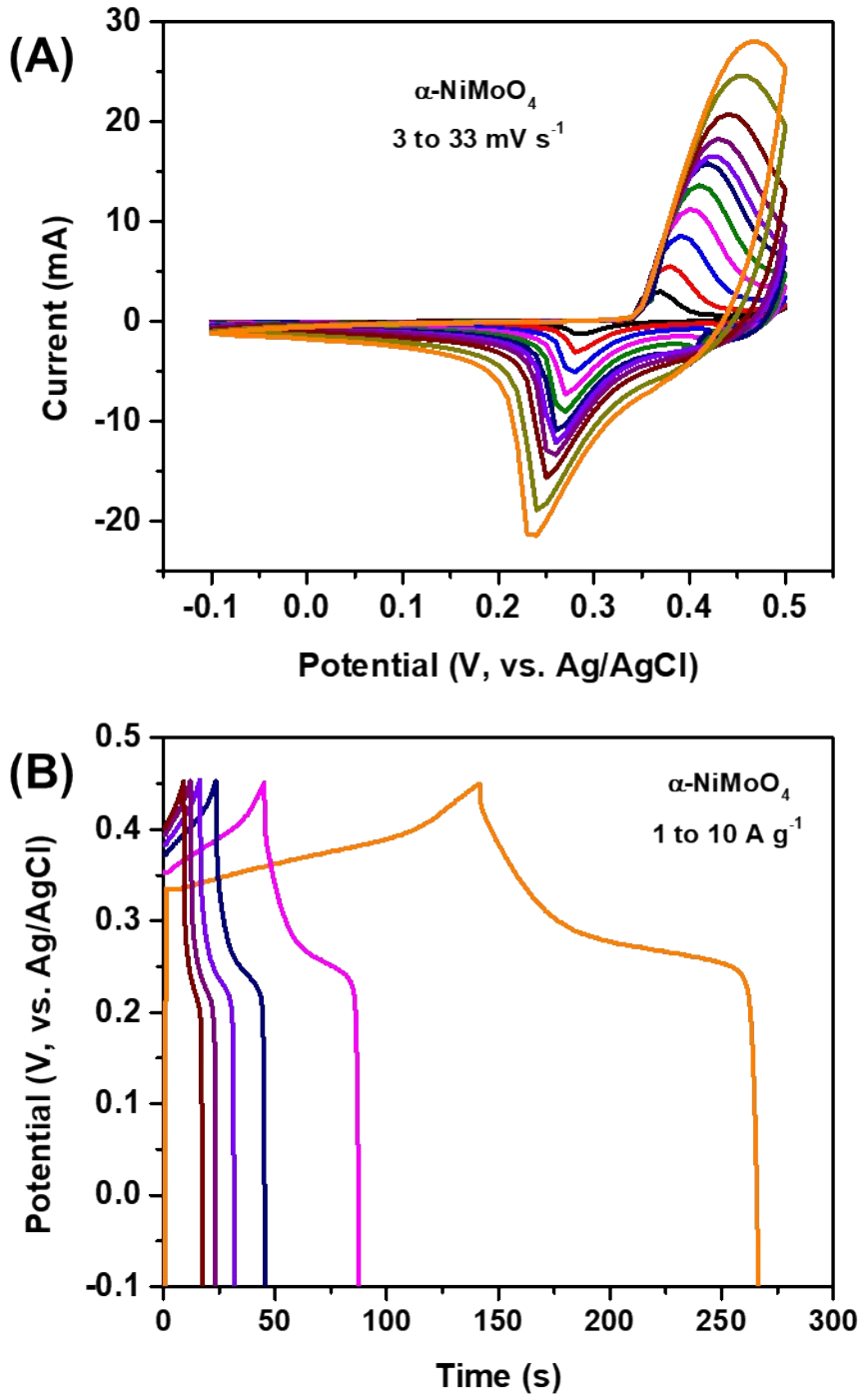

Fig. S2. (A) CV curves and (B) GCD profiles of the α-$NiMoO_4$@CC electrode at different scan rates (3 to 33 mV s^{-1}) and current densities (1 to 10 A g^{-1}), respectively.

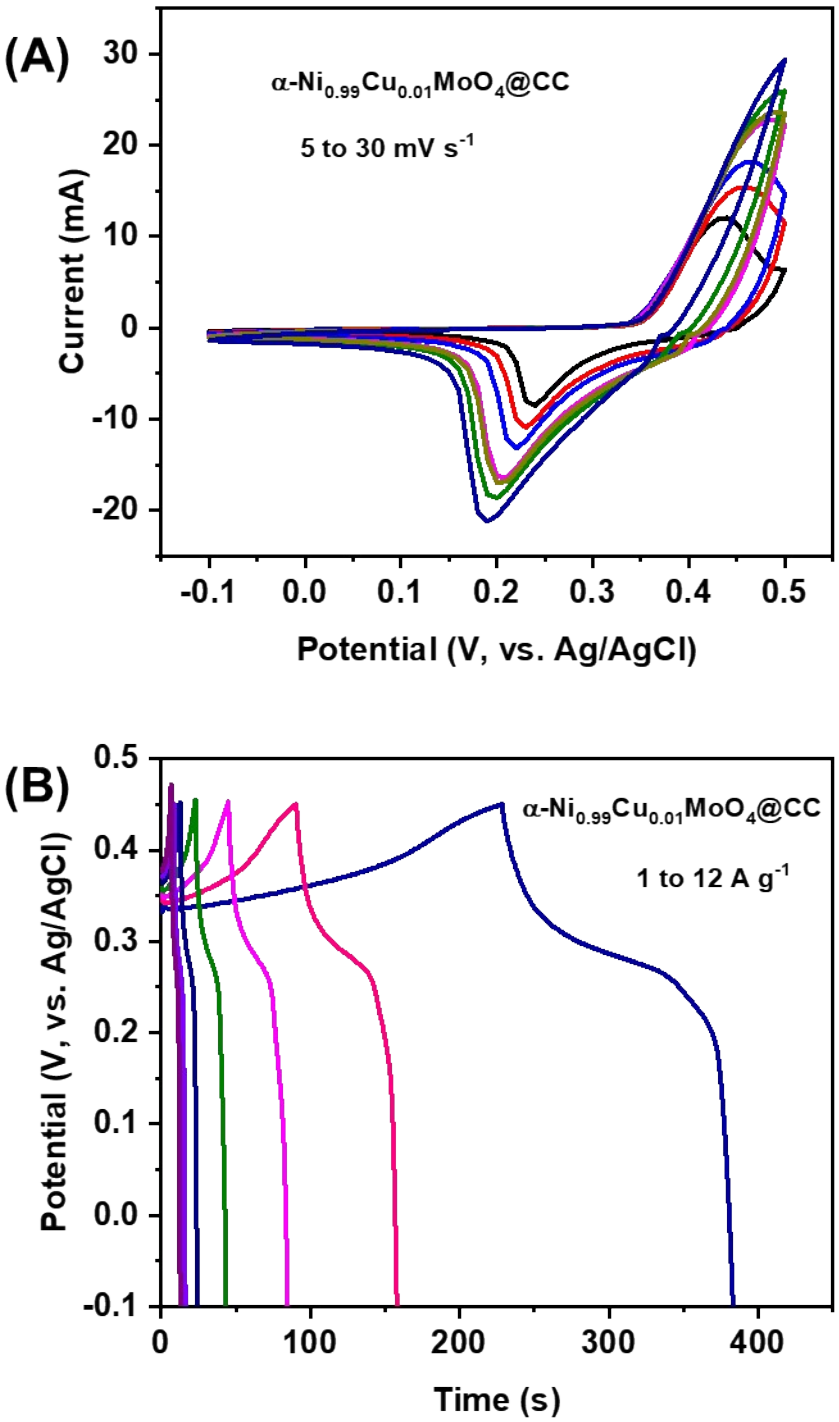

Fig. S3. (A) CV curves and (B) GCD profiles of the α-$Ni_{0.99}Cu_{0.01}MoO_4$@CC electrode at different scan rates (3 to 30 mV s^{-1}) and current densities (1 to 12 A g^{-1}), respectively.

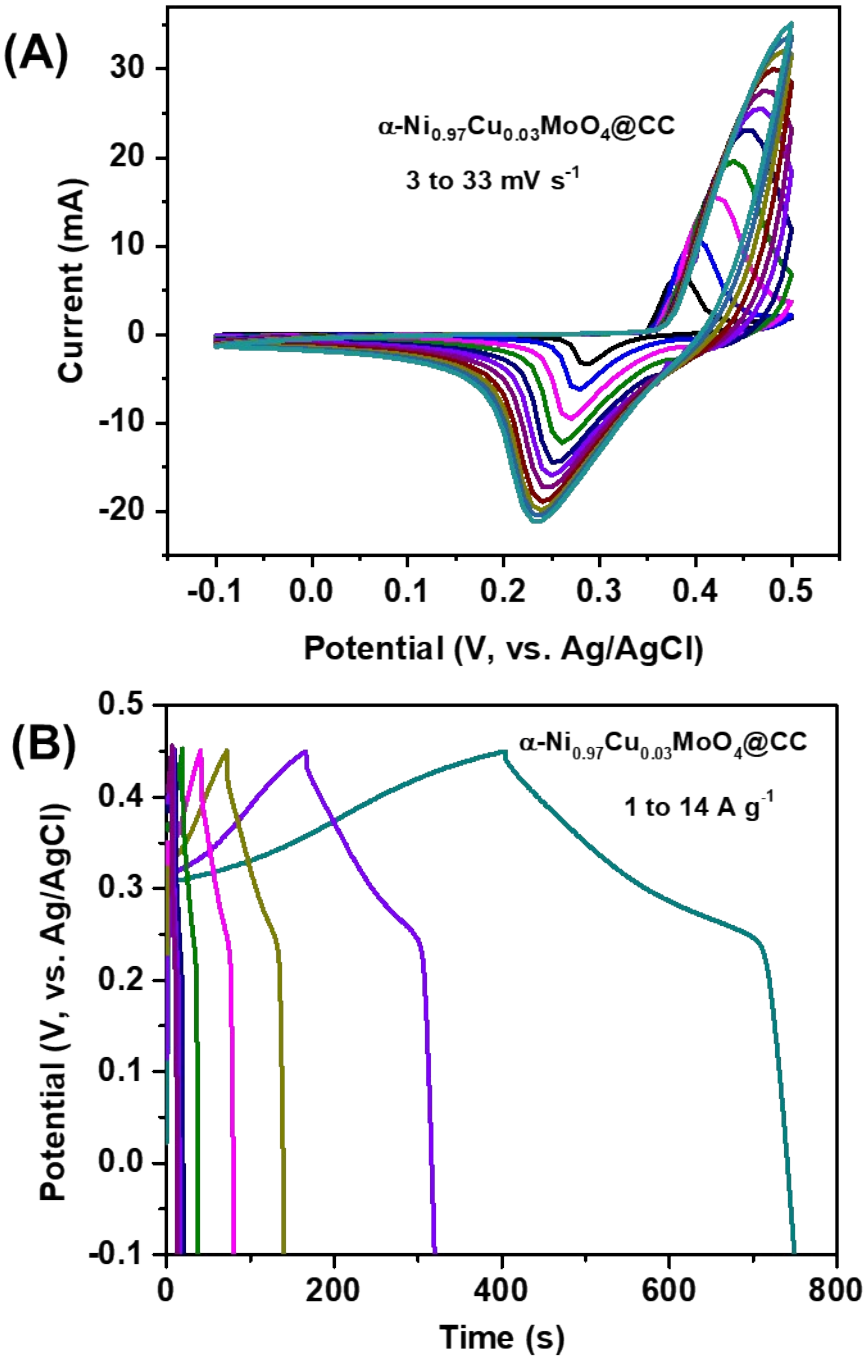

Fig. S4. (A) CV curves and (B) GCD profiles of the α-$Ni_{0.97}Cu_{0.03}MoO_4$@CC electrode at different scan rates (3 to 33 mV s^{-1}) and current densities (1 to 12 A g^{-1}), respectively.

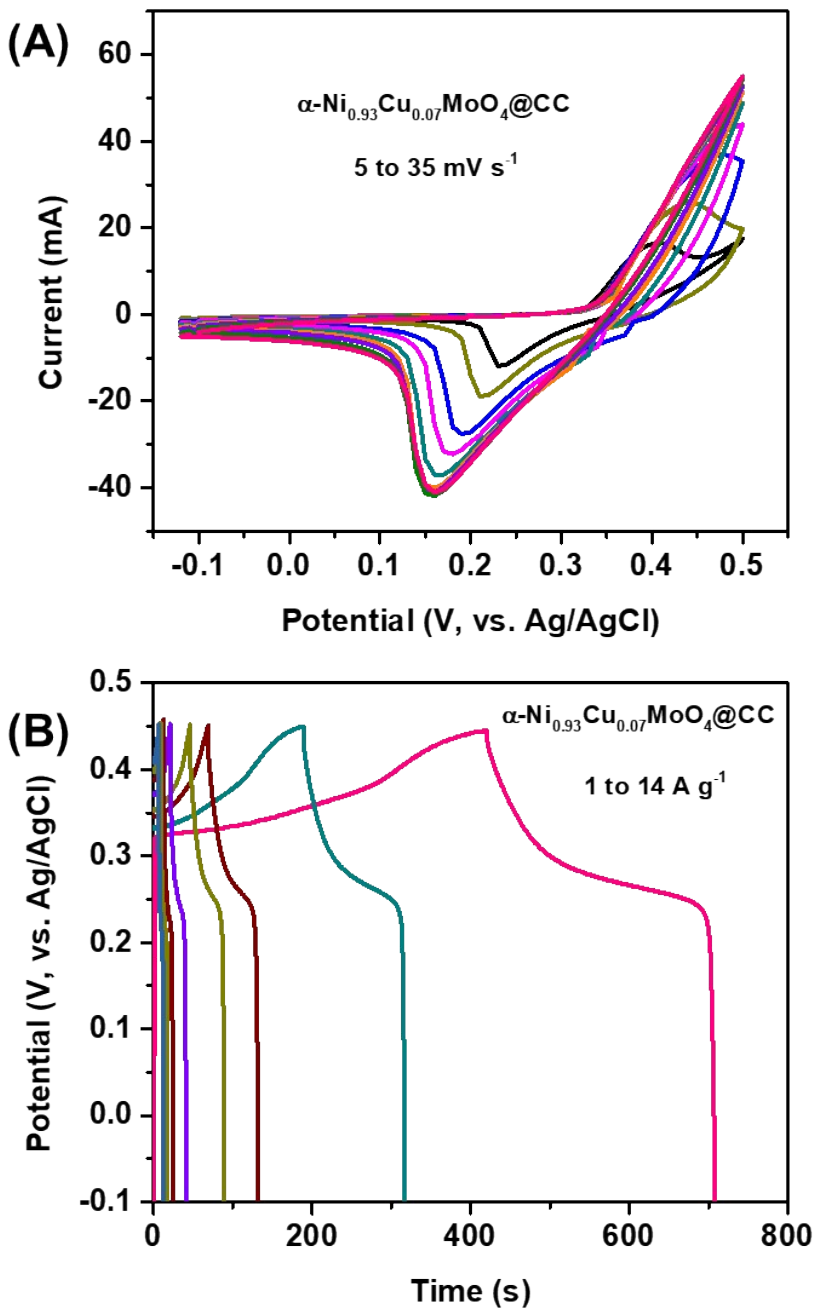

Fig. S5. (A) CV curves and (B) GCD profiles of the α-$Ni_{0.93}Cu_{0.07}MoO_4$@CC electrode at different scan rates (3 to 33 mV s^{-1}) and current densities (1 to 12 A g^{-1}), respectively.

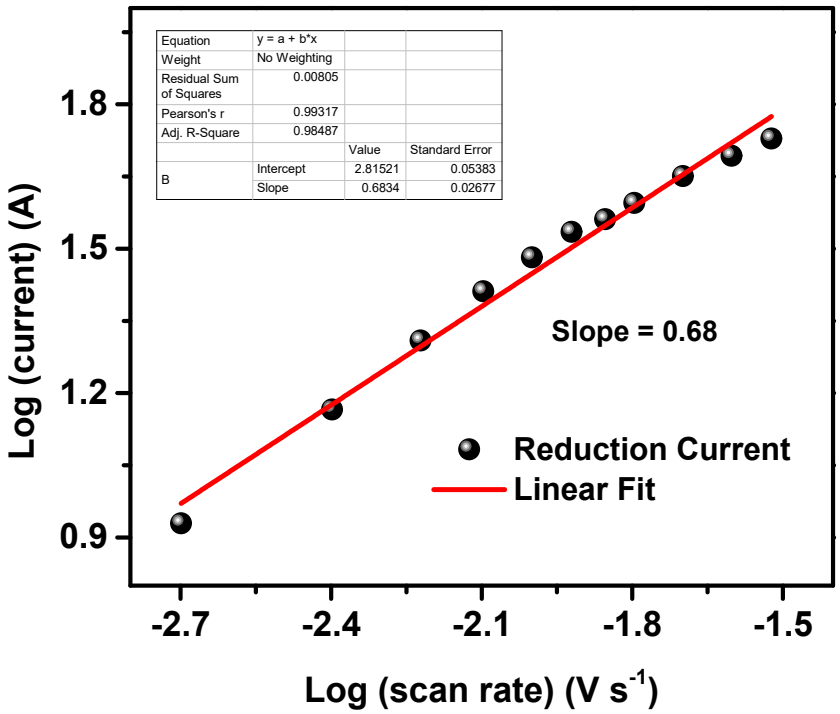

Fig. S6. Calculated *b* value of the α-$Ni_{0.95}Cu_{0.05}MoO_4$@CC electrode from the cathodic peak currents.

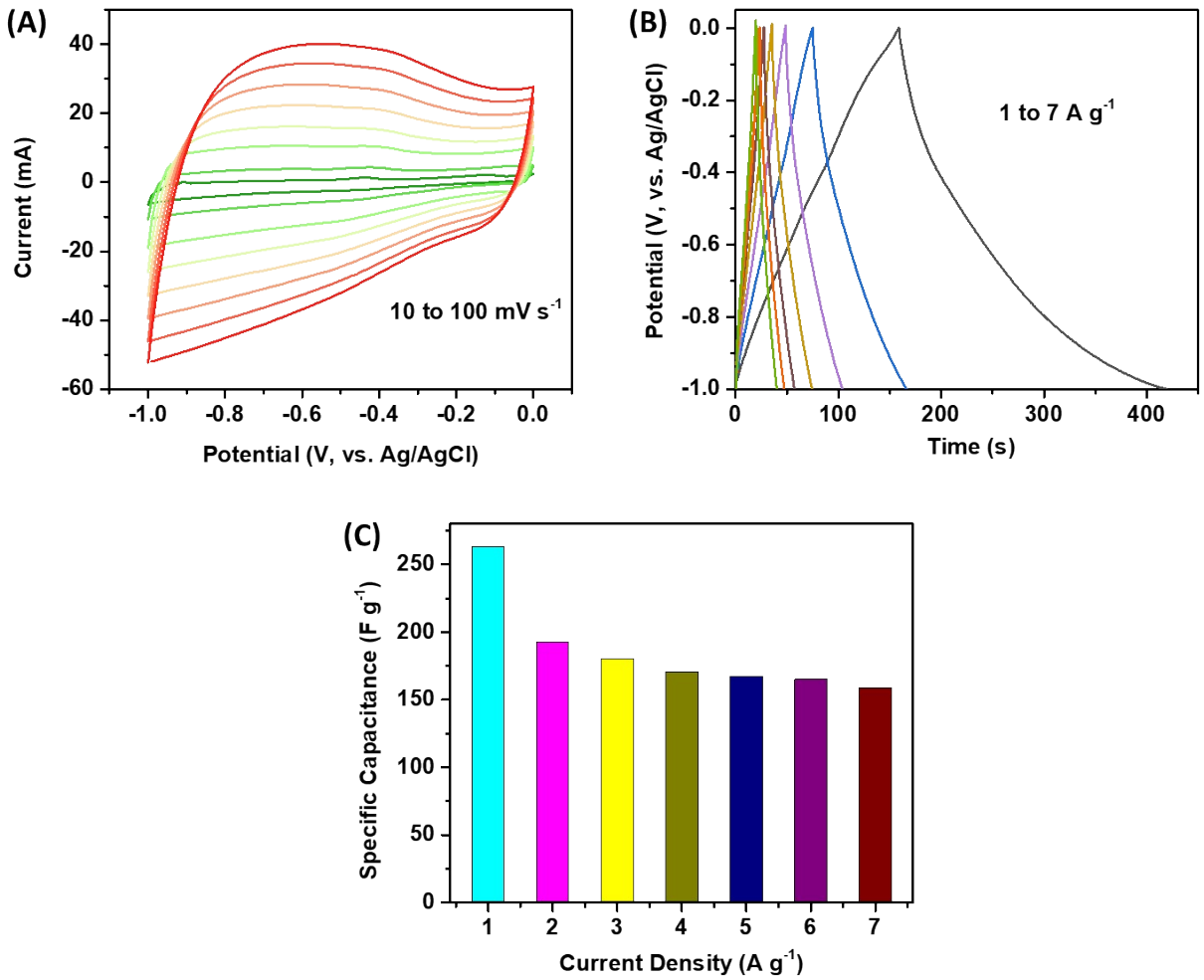

Fig. S7. (A) CV curves at different scan rates (10 to 100 mV s^{-1}), (B) GCD curves at different current densities (1 to 7 A g^{-1}), and (C) C_s values of the AC@CC electrode.

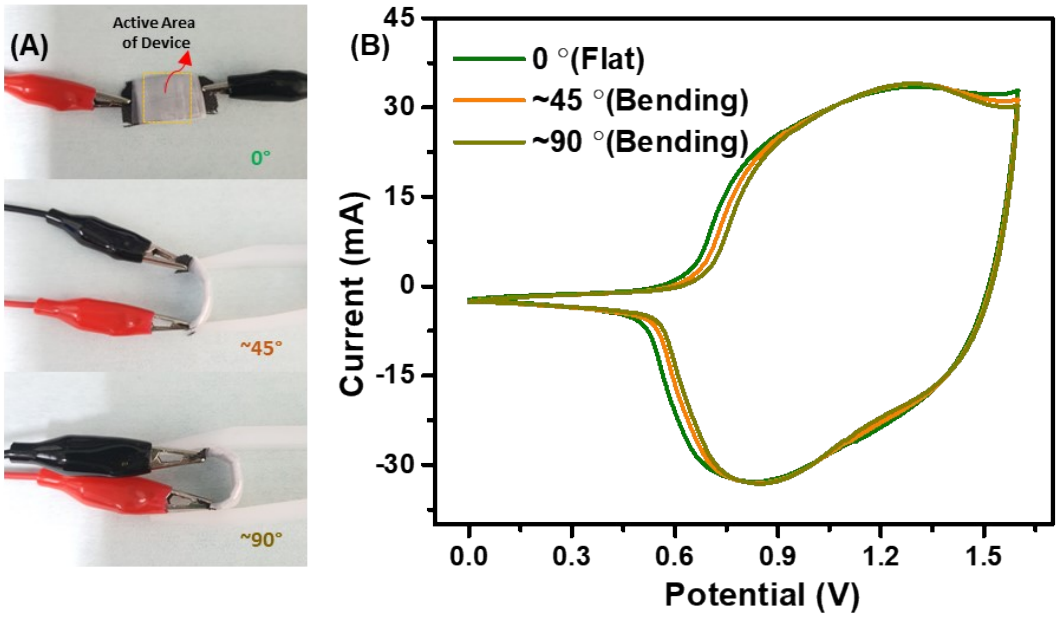

Fig. S8. (A) Digital photographic images. (B) CV curves (at 50 mV s^{-1}) of the α-$Ni_{0.95}Cu_{0.05}MoO_4$@CC//AC@CC FHS device in flat and bending positions.